Time evolution of a quenched binary alloy. IV. Computer simulation of a three-dimensional model system*

Amit Sur and Joel L. Lebowitz
Belfer Graduate School of Science, Yeshiva University, New York, New York 10033

J. Marro
Departamento de Física Teórica, Universidad de Barcelona, Barcelona-14, Spain and Belfer Graduate School of Science, Yeshiva University, New York, New York 10033

M. H. Kalos
Courant Institute of Mathematical Sciences, New York University, New York, New York 10012

(Received 27 September 1976)

We present results of computer simulations of the time evolution of a model binary alloy following quenching. Our model system is a simple cubic lattice each site of which is occupied by either an A or a B atom. There is a nearest-neighbor interaction which favors segregation into an A-rich and a B-rich phase at a point inside the two-phase region. Starting from a random configuration the system is quenched to and evolves at a finite temperature T as exchanges between atoms on nearest-neighbor sites are allowed to take place. In our present study, a lattice having a 20% concentration of A atoms ($\bar{n}_A = 0.20$), was quenched to temperatures $T = 0.6\,T_c$ and $T = 0.9\,T_c$, inside the two-phase region, and to $T = 1.1\,T_c$. We study the evolution of the spherically averaged structure function $S(k,t)$, the energy, and various cluster properties, and compare our results with relevant theoretical predictions. We also compare the late time cluster distributions of small clusters for $T = 0.6\,T_c$ and $T = 0.9\,T_c$ with the equilibrium cluster distributions for corresponding temperatures on the coexistence curve (namely, $\bar{n}_A = 0.0146$ at $T = 0.6\,T_c$, and $\bar{n}_A = 0.1272$ at $T = 0.9\,T_c$). This shows that the phase segregation at $T = 0.6\,T_c$ takes place in two distinct stages (i) a "rapid" condensation of the A atoms into "liquid" drops and a "gas" phase consisting of monomers, dimers, etc., and (ii) a "slow" growth of the droplets. At $T = 0.9\,T_c$ (which is well inside the "classical" metastable region) such a segregation still seems to take place but at a slower rate.

I. INTRODUCTION

The quenching of an alloy from a completely miscible initial state to a point inside the two-phase region (where the equilibrium state corresponds to the coexistence of two segregated phases) is followed by a process of phase segregation. In the classical theory of this process it is customary to think of a "spinodal curve"[1] which separates metastable from unstable parts of the two-phase region. When the quench is to a point inside the spinodal curve the phase separation is assumed to take place by long-wavelength fluctuations and termed "spinodal decomposition."[2] This is characterized experimentally by the formation of a uniformly dispersed precipitate and subsequent coarsening of the grains.[2,3] If, however, the quench is to a state between the coexistence curve and the spinodal curve, the system is thought to be stable with respect to these delocalized fluctuations, but still unstable with respect to strong localized fluctuations, i.e., nucleus formation. In this case phase separation is assumed to occur by homogeneous nucleation.[4]

The delineation of these two regions is based, in the linearized Cahn-Hilliard theory,[2] on a van der Waals–like free energy density whose second density derivative vanishes on the spinodal line. Not surprisingly the actual situation is much more complicated than that implied in this simple picture. In particular there is no evidence for a sharp separation between the two regions. Rather there appear to be gradual changes as one goes away from the center of the spinodal region towards the coexistence lines. As the coexistence line is approached the rate of segregation becomes slower and slower eventually becoming vanishingly small on any observable time scale: one is then in the metastable region.[5]

In order to understand the kinetics of the phase segregation process in a quantitative microscopic manner we have been carrying out computer simulations of a model binary alloy in two and three dimensions. The time evolution of a quenched A-B alloy with equal concentration of A and B atoms was studied by Bortz *et al.*[6] for a square lattice and by Marro *et al.*[7] for a simple cubic lattice (hereafter referred to as I and II, respectively). Further studies on the square lattice were made by Rao *et al.*[8] (hereafter referred to as III) where the case of a 20% concentration of A atoms was also considered and a study was

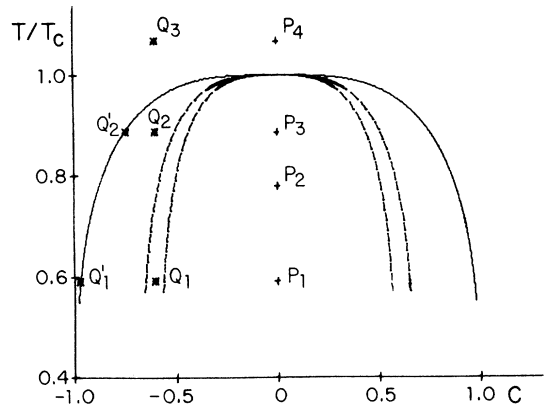

FIG. 1. Phase diagram for the A-B alloy or for the infinite three-dimensional Ising model. The coexistence curve (solid line) is drawn according to a low-temperature series expansion (Ref. 12). The "spinodal" curves are drawn assuming a local-free-energy density of the form $f(C)=-\alpha C^2+\beta C^4+\gamma C^6$ below T_c. $\gamma=0$ corresponds to the inner dashed line ("classical spinodal") and $\beta=0$ to the outer dashed line (Ref. 10).

made of the cluster kinetics.

In these simulations the sites of the lattice are occupied by either an A or a B atom, while the interaction energy U is assumed to be of the form

$$U=-J\sum{}'\eta(\vec{\mathbf{r}}_i)\eta(\vec{\mathbf{r}}_j), \tag{1}$$

where $J>0$, and $\eta(\vec{\mathbf{r}}_i)=\pm 1$, according to whether there is an A or a B atom present at site i. The sum in (1) is over all nearest-neighbor pairs in our cubical sample containing N (27 000 or 125 000) sites with periodic boundary conditions. This system is isomorphic to the spin-$\frac{1}{2}$ Ising model of a magnet,[9] where the spin at each site can point "up" (A particle) or "down" (B particle) and to the lattice-gas model for fluids, where each site can be either[9] occupied (A particle) or empty (B particle). The concentration of A atoms is $\bar{n}_A=\frac{1}{2}(C+1)$, where $C=N^{-1}\sum_i\eta(\vec{\mathbf{r}}_i)$ is the average magnetization in the lattice. The phase diagram for this system is given in Fig 1 (cf. II). Also shown in Fig. 1 are two "spinodal lines": the classical one, corresponding to a local-free-energy density $f(C)=-\alpha C^2+\beta C^4$ and one based on $f(C)=-\alpha C^2+\gamma C^6$ suggested by Amit and Fisk and Widom[10]; α,β,γ are positive constants.

Starting from a random configuration (which corresponds to an initial temperature $T_0=\infty$) the system is quenched instantaneously to a lower temperature $T=(k_B\beta)^{-1}$, i.e., it is allowed to evolve by exchanges of *nearest-neighbor* atoms which take place according to a Markovian transition probability per unit time given by

$$P_{ij}=\alpha e^{-\beta\Delta U_{ij}}/(1+e^{-\beta\Delta U_{ij}}). \tag{2}$$

Here ΔU_{ij} is the change in energy of the system which would result from the exchange and α^{-1} is the unit of time. In a real system the energy for exchange is supplied by the phonons which makes α strongly temperature dependent: $\alpha\sim\nu_0 e^{-\phi/kT}$, where ν_0 is an "attempt" frequency and ϕ is a potential barrier which has to be overcome and is here assumed independent of configurations.

The linearized Cahn-Hilliard theory of spinodal decomposition predicts a simple exponential growth in time for the structure function $S(\vec{\mathbf{k}},t)$, defined as the Fourier transform of the spatial correlation $N^{-1}\sum_i\eta(\vec{\mathbf{r}}_i)\eta(\vec{\mathbf{r}}_i+\vec{\mathbf{r}})$ following a quench inside the spinodal. In contrast, our previous studies have shown no such exponential growth. We could instead represent the growth of the peak of $S(\vec{\mathbf{k}},t)$ by a fractional power law, while the position of the peak was observed to shift towards smaller values of k, as the system evolves in time. This behavior is similar to some experimental observations[3(a)] and the results in II were in good agreement with the theory of Langer *et al.*[11]

The presence of vacancies is assumed to play an important role in the diffusion and segregation of species in binary alloys. We have recently tested the sensitivity of our results to the details of the model by carrying out computations in which some sites of the lattice were empty. This corresponds to having $\eta(\vec{\mathbf{r}}_i)$ in Eq. (1) take on the values $1,0,-1$. The time evolution now takes place by having an A or B atom exchange positions with a neighboring vacancy with a probability given also by (2). Preliminary results for the case 49% A atoms, 49% B atoms, 2% vacancies, $T=0.59T_c$, indicate no qualitative change in the development of $S(\vec{\mathbf{k}},t)$.

The phase points studied in II correspond to an alloy containing 50% A atoms and 50% B atoms ($C=0$) arranged on a simple cubic lattice; they are denoted by $P_1(4\beta J=1.5, T=0.59T_c)$, $P_2(4\beta J=1.137, T=0.78T_c)$, $P_3(4\beta J=1, T=0.89T_c)$, and $P_4(4\beta J=0.83, T=1.07T_c)$ in Fig. 1; $T_c=4.510J/k_B$ in our model system.[12] Here we extend the computations to an alloy containing 20% A atoms and 80% B atoms ($C=-0.6$) which allows for a study of cluster formation in the minority (A) phase surrounded by the "matrix" (B) phase. We investigate the time evolution following quenching to different temperatures; the corresponding points in the phase diagram are marked: $Q_1(T=0.59T_c)$, $Q_2(T=0.89T_c)$, and $Q_3(T=1.07T_c)$ in Fig. 1. We first describe the time dependence of $S(\vec{\mathbf{k}},t)$ and the energy, and compare our results with relevant computations of II. We then study the cluster properties of our system and compare the results for the segregated (gas) phase of Q_1 and Q_2 with the

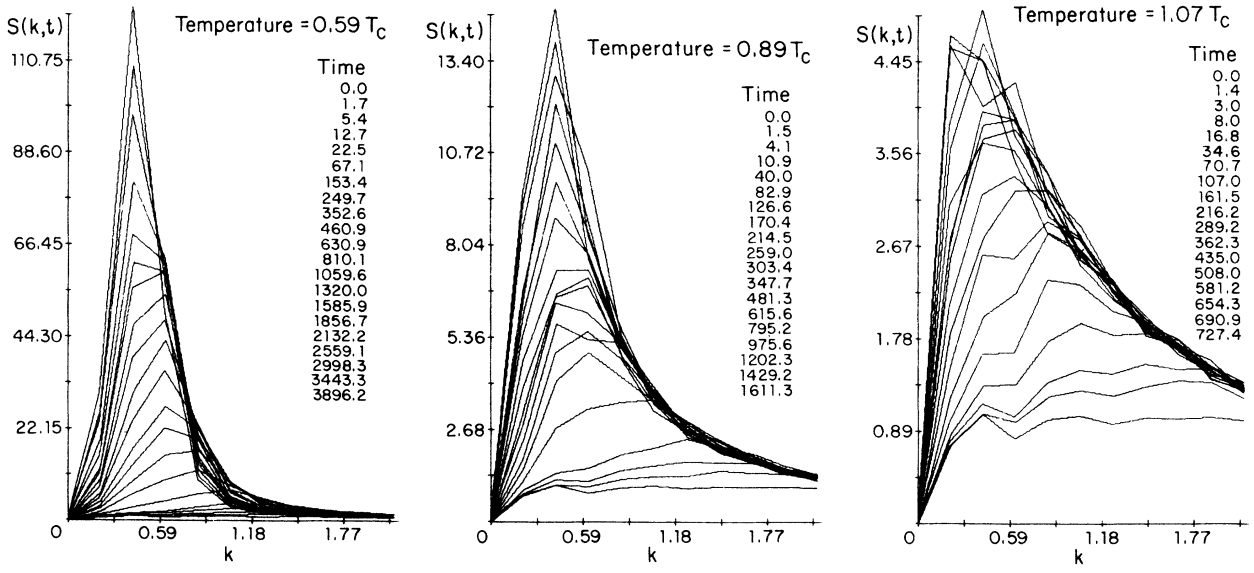

FIG. 2. (a)–(c) Development with time of $S(k,t)$ vs k at different temperatures, corresponding to the points Q_1, Q_2, and Q_3, respectively, in Fig. 1. Increasing values of the time in units of α^{-1} correspond to the different graphs from the bottom of each picture to the top.

observed equilibrium cluster properties on the coexistence curve Q_1' ($\bar{n}_A = 0.0146$ at $T = 0.59T_c$) and Q_2' ($\bar{n}_A = 0.127$ at $T = 0.89T_c$).

II. TIME EVOLUTION OF THE STRUCTURE FUNCTION AND THE ENERGY

The spherically averaged structure function $S(k,t)$ is plotted in Fig. 2 as a function of k for different values of time after quenching to Q_1, Q_2, and Q_3, respectively. We define $S(k,t)$ as

$$S(k,t) = \sum' S(\vec{k},t) \Big/ \sum' 1,$$

where $\vec{k} = (2/L)\pi\vec{\mu}$, $\mu_i = 0,1,2,\ldots,L-1$, $(L = N^{1/3})$, and the sum $\sum'$ goes over all values of $\vec{k}$ such that $(2/L)\pi\mu \leq |\vec{k}| \leq (2/L)\pi(\mu+1)$. In the actual simulation we computed $S(\vec{k},t)$ for $\vec{k}$ in one octant of the reciprocal lattice up to $|\vec{k}| = 2/3\pi$.

From Fig. 1, we see that Q_1 ($\bar{n}_A = 0.2, T = 0.6T_c$) is slightly outside the classical spinodal line but inside the "new" spinodal line suggested by Amit and by Fisk and Widom.[10] Using the classical form of the free energy the linearized Cahn-Hilliard theory predicts no decomposition at all for this case, whereas Langer *et al.*[11] predict a broad but well-defined peak for $S(k,t)$. This peak according to the latter authors will have considerably less intensity than that at P_1, which is at the same temperature but has $\bar{n}_A = 0.5$ and is thus at the center of the spinodal region. They also predict a "common tail" for large k. The observed $S(k,t)$ [Fig. 2(a)] however is like that observed for P_1, as shown in Fig. 2 of II, and similar to the experimental result in Al-Zn alloy for 22% Zn in that the tail as well as the peak is changing with time. This gives rise to the "crossovers" of the curves in Fig. 2(a) characteristic of Langer's theory in the spinodal region.

The point Q_2 lies almost in the center of the classical metastable region of the phase diagram (see Fig. 1). The observed $S(k,t)$ for this point as shown in Fig. 2(b) is rather similar to that for P_4 ($\bar{n}_A = 0.5, T = 1.1T_c$) displayed in Fig. 5 of II. Here we find that, after an initial growth for large values of k, $S(k,t)$ quickly decays to a steady value giving rise to a common tail for all the curves in Fig. 2(b). Thus, using the behavior of $S(k,t)$ for short wavelengths as a criterion, we would say that Q_2 is outside the spinodal region, as also is the case in Fig. 1. This is, however, only one possible consideration and other criteria might yield a different answer, as we shall see in examining the cluster distributions.

The point Q_3 is outside the coexistence region yet rather close to T_c so that significant "local ordering" can take place. This gives rise to an early time behavior of $S(k,t)$ similar to that for coarsening. This has been observed in II for P_4. Our result for Q_3 [see Fig. 2(c)] is qualitatively similar to that for P_4, but the intensity is lower and more comparable to that observed recently[13]

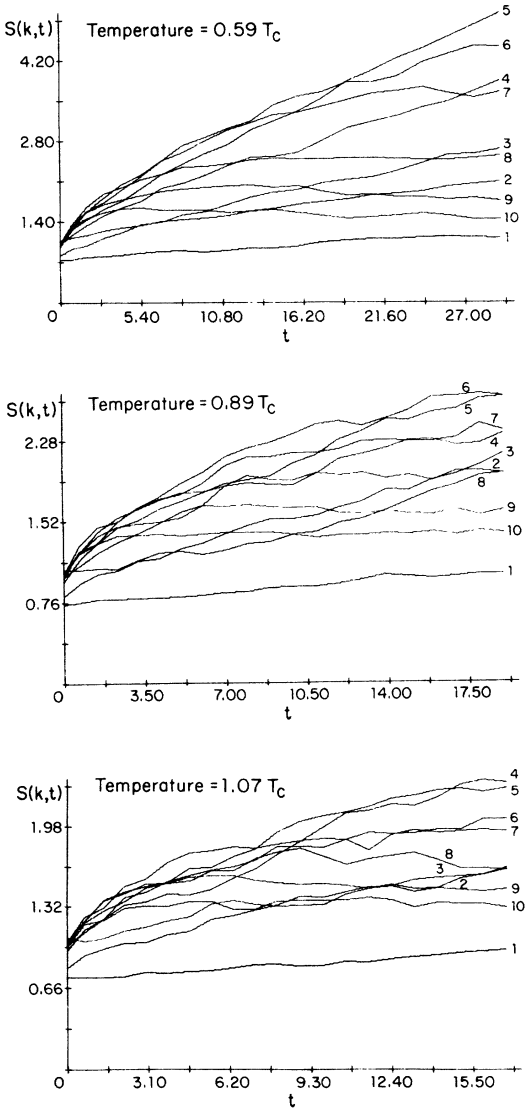

FIGS. 3. (a)–(c) Early-time evolution of $S(k,t)$ as a function of time for different values of k at different temperatures corresponding to the points Q_1, Q_2, and Q_3, respectively, in Fig. 1. At the end of each line is shown the corresponding value of $\mu = 30k/2\pi$.

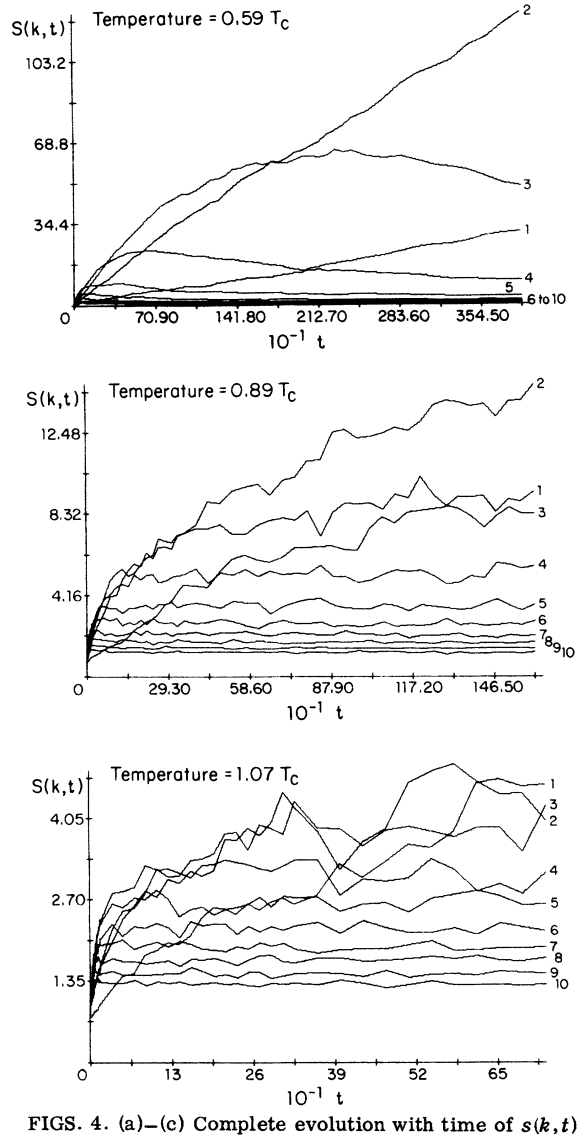

FIGS. 4. (a)–(c) Complete evolution with time of $s(k,t)$ for different values of k at different temperatures, corresponding to the points Q_1, Q_2, and Q_3 in Fig. 1, respectively.

for $\bar{n}_A = 0.5, T = 1.5T_c$. We believe that our late time values for $S(k)$ are those of the equilibrium system.

In Figs. 3 and 4 $S(k,t)$ is plotted as a function of time for different values of k, the early time behavior being shown in Figs. 3(a)–3(c), while the late time situation is displayed in Figs. 4(a)–4(c). A study of these figures shows that there is no regime where $S(k,t)$ grows exponentially. We see that at Q_1 [see Figs. 3(a) and 4(a)] $S(k,t)$ initially grows with time, reaches a peak, and then decays. The decay starts at successively earlier times as k increases. This corresponds to the crossover behavior discussed earlier. For the smallest-k values studied this peak is never reached during the course of the experiment. For Q_2 [see Figs. 3(b) and 4(b)] we find a behavior similar to that for P_3 (see Fig. 11 in II). Here $S(k,t)$ continues to grow as time increases until it reaches a maximum value at t', and then appears to remain stationary. The maximum value as well as t' decreases as k increases. This corresponds to the common tail in Fig. 2(b). Similar results are obtained for Q_3 [see Figs. 3(c) and 4(c)] where

TABLE I. Values of a, a', and a'' for different points in the phase diagram assuming a power-law temporal evolution for the first moment of $S(k,t)$, $\bar{k}(t) \sim t^{-a}$, the location of the peak, $k_m(t) \sim t^{-a'}$, and the height of the peak, $S(k_m,t) \sim t^{a''}$.

	$\bar{n}_A = 0.20$		
	$T = 0.6T_c$	$T = 0.9T_c$	$T = 1.1T_c$
a	0.19	0.12	0.07
a'	0.20	0.16	...
a''	0.70	0.41	0.24

the system actually goes to equilibrium in our simulations.

Following II, we characterize the time evolution of $S(k,t)$ by (a) $\bar{k}(t)$, the first moment of $S(k,t)$; (b) the location of the peak $k_m(t)$; and (c) the height of the peak $S[k_m(t),t]$, using a parabolic fit for three values of k around k_m. Setting $\bar{k}(t) \sim (t+10)^{-a}$, $k_m(t) \sim (t+10)^{-a'}$, $S(k_m,t) \sim (t+10)^{a''}$, we find values of a, a', a'' listed in Table I. Binder and Stauffer[14] predict $a'' = 3a'$ and $a' = \frac{1}{6}$ at "low temperatures," $a' = \frac{1}{4}$ for $T \approx T_c$, and $a' = \frac{1}{2}$ for $T > T_c$. Only the first of the predictions is in reasonable agreement with our results for Q_1. A comparison of the exponents displayed in Table I ($\bar{n}_A = 0.20$) with those given in Table II of II ($\bar{n}_A = 0.50$) shows that the results are rather similar for Q_1 and P_1, and for Q_2 and P_4. We also find that results for Q_3 are similar to that for $T = 1.5T_c$ and $\bar{n}_A = 0.5$ as given in Ref. 13. The difference between values for a and a' in Table I for Q_2, seems to be due to the fact that $S(k,t)$ for this point is not so sharply peaked as for Q_1 near its maximum. This is even more so for Q_3 where we could not determine a meaningful value for a'.

We have also studied the shape of $S(k,t)$ for $k > k_m(t)$ by fitting it to the expression

$$S(k,t) \sim c_1(t)/[k^2 + c_2(t)]. \tag{3}$$

We find that the absolute value of $c_2(t)$ decreases with time during the experiment; $c_2(t)$ itself is always positive for high temperatures (Q_2 and Q_3), while it remains negative for Q_1 as one would expect for a system undergoing decomposition. The values of $c_2(t)$ corresponding to the latest times in our simulation are, for increasing temperatures -0.38, 0.39, and 1.74, respectively. The quantity $c_1(t)$ in Eq. (3) markedly decreases with time for Q_1, corresponding to the crossover of the tail in Fig. 2(a), while it decreases very slowly for Q_2 and remains stationary for Q_3 giving rise to a common tail in these two cases [see Figs. 2(b) and 2(c)]. Our latest values for c_1 are 2.27, 5.56, and 7.69 for increasing temperatures, respectively. The rms fluctuations for the numbers quoted above are in every case around 2%.

TABLE II. Values for different points in the phase diagram for the equilibrium value of $N_{AB}/N = u$ as computed from the relation (see II) $u_\infty(T) \simeq u_I(0)\sigma(T) + u_p(T)$ for $T < T_c$, where $u_I(0)$ stands for the value of u or "surface area" at $T = 0$, $\sigma(T)$ for the surface tension (taken from Monte Carlo computations Ref. 16) and $u_p(T)$ is the equilibrium value of u in the pure phase (estimated by Padé approximants, Ref. 15). Our experimental equilibrium values for u are also shown.

		$u_\infty(T)$	
T/T_c	$\bar{n}_A$	Expt.	Theor.
0.6	0.20	...	0.18
0.6	0.0146	0.082	0.08
0.9	0.20	...	0.65
0.9	0.127	0.55	0.53
1.1	0.20	0.79	...

We have investigated the asymptotic time behavior of the quantity $u = N_{AB}/N$, where N_{AB} is the number of A-B bonds in the system, u is related to the energy per site U/N defined in Eq. (1) by $U/N = (2u - 3)J$. The equilibrium value of u, which we denote by $u_\infty(T)$, can be obtained for the point Q_3 in the one-phase region, from our computer experiments when the system reaches its equilibrium state.[13] For points in the two-phase region, $u_\infty(T)$ was obtained approximately [see Eq. (3.1) in II] from estimates of the interfacial energy and the equilibrium energy in the pure phase; the latter were taken from our computer experiments on the coexistence curve (Q_1' and Q_2') which are in good agreement with the values obtained from low- and high-temperature expansions for the specific heat[15] (see Table II for a comparison). As in our previous studies, the time dependence, for the range of time studied, can be put in the form,

$$u \sim t^{-b}, \quad u - u_\infty(T) \sim t^{-b'}. \tag{4}$$

The values of b and b' are given in Table III. A comparison of the present results with those in II (Table I), shows once again the exponents for

TABLE III. Values for different points in the phase diagram of the parameters characterizing the time evolution of the energy of the system [see Eq. (4)] assuming a power-law behavior.

	$\bar{n}_A = 0.20$		
	$T = 0.6T_c$	$T = 0.9T_c$	$T = 1.1T_c$
b	0.16	0.02	...
b'	0.28	0.14	1.0–1.1

Q_1 and Q_2 are rather close in value to those for P_1 and P_4, with the exception that b' for Q_2 is rather low. Our result for Q_1 seems to be in good agreement with that of Binder and Stauffer[14] ($b' = \frac{1}{6}$) but not so at other points. Clearly however we might not yet be in the asymptotic regime and the power-law representations are just one of several possible ways of analyzing the data.

As mentioned earlier the theoretical predictions of Langer *et al.*[11] for $S(k,t)$ are in very good agreement with our results in II for $\bar{n}_A = 0.5$. In that theory it is assumed that $S(k,t)$ obeys scaling laws in the vicinity of the critical temperature, $T \lesssim T_c$. The function $S(k,t)$ may then be expressed in a universal form $S(q,\tau)$, using dimensionless variables q and τ (cf. Ref. 11 and II). We compared our results for Q_1 and Q_2 with those obtained from the theory proposed by Langer *et al.*[11] with $x_0 = 0.617$ and 0.805, respectively, where $x_0 = (\bar{n}_A - 0.5)/(\bar{n}_A^{\text{coex}} - 0.5)$. We found, not surprisingly, that scaling no longer holds for our concentrations and temperatures. Although the theory approximately predicts the position of the peak, its predictions for $S(k,t)$ are typically smaller than the observed values by a factor of $\frac{1}{2}$. Indeed our observations for Q_1 and Q_2 are in reasonable agreement with computations in Ref. 11 for $x_0 = 0$ and $x_0 = 1/\sqrt{3}$, respectively, instead of a larger values of x_0 they should correspond to. This disagreement may be due primarily to the use, in Ref. 11, of a quartic polynomial for the free-energy density below T_c, or it may indicate the necessity for a new theory to describe the behavior of $S(k,t)$ when the system is quenched to points close to the coexistence line. It would certainly be useful to carry out computations on Langer's theory with a more general free energy function. As already mentioned, using a quadratic plus sixth-order term in the free energy[10] makes the point Q_1 lie in the spinodal region, and it is possible that Langer's theory with such a free energy would be consistent with our observations. It would be even more interesting to understand what is happening at Q_2 where, as we shall see in Sec. III, the system is undergoing phase segregation at a very slow rate.

III. CLUSTER ANALYSIS

We describe now our observations concerning the formation of "clusters" of A atoms following quenching. A cluster C is defined as a group of A atoms linked together by nearest-neighbor bonds. Each cluster C was characterized in our computations by k, the number of sites in the cluster, and s, the surface area, defined as the total number of AB bonds incident on C_{ks}. For

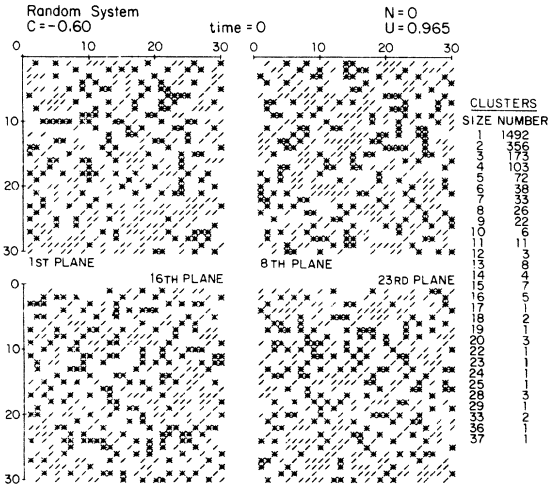

FIG. 5. Snapshot pictures of four 30×30 planes of the random system ($T = \infty$); i.e., the initial configuration corresponding to one of the runs. U in the figure stands for u; N for the number of exchanges. Note the meaning of the different symbols in Figs. 5–8: ⊙ denotes an "interior" A particle (all of whose neighbors are A particles), $*$ denotes a noninterior A particle, / denotes an interior B particle, and the absence of any symbols in the lattice, a noninterior B particle. The corresponding cluster distribution in the system is also shown.

our model system, s corresponds to the energy of the cluster C_{ks}, i.e.,

$$u = N^{-1} \sum_{s,k} s N_{ks} ,$$

where N_{ks} is the number of clusters of type C_{ks}. The computer is programmed to list, at prescribed times, $N_k = \sum_s N_{ks}$, the total number of clusters of size k and $s_k = \sum_s s N_{ks}$, the total surface area of all clusters of size k.

We first study the cluster properties qualitatively with the help of snapshot pictures of four 30×30 planes of the system, taken from one of our runs, shown in Figs. 5–8. (See figure captions for the interpretation of the different symbols.) The cluster distribution N_k for the system at the time of the snapshots is also shown in each of the graphs. The initial random state is shown in Fig. 5. We note that in the initial state there are no "interior" A particles, and the largest cluster size is only 37.

Figs. 6(a) and 6(b) show evolution at Q_1 where the final state should be one of coexistence of two phases. After a rather short time, the system is characterized by the appearance of (i) a stabilized phase containing small clusters ($k \leq 10$) (we identify this as the gas phase as discussed later); (ii) one or two giant clusters containing about (40–60)% of the A particles present in the system; and (iii)

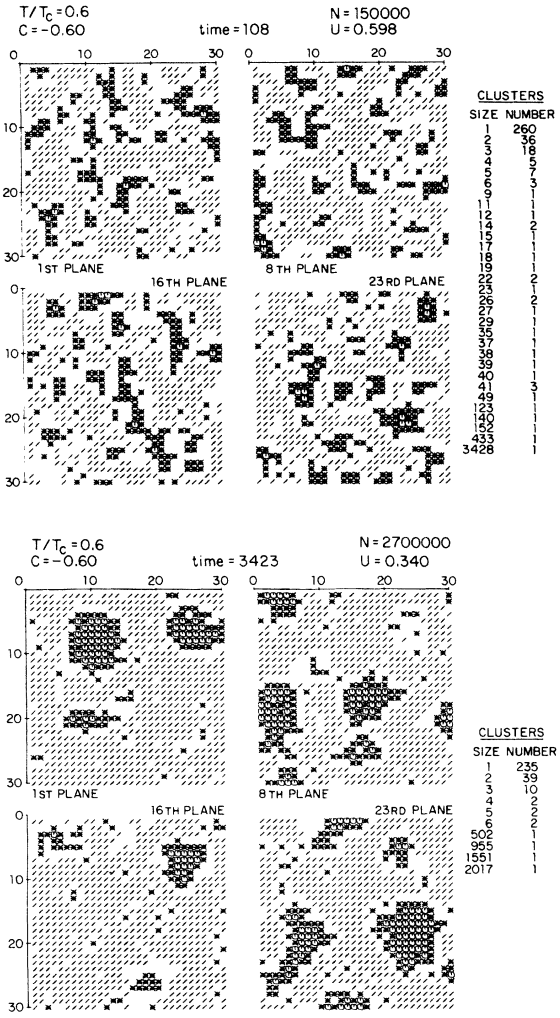

FIG. 6. Same as in Fig. 5 for $T = 0.6T_c$ at two different stages of the evolution. The value of the time, shown in the figures, is in units of α^{-1}. See Sec. III for details.

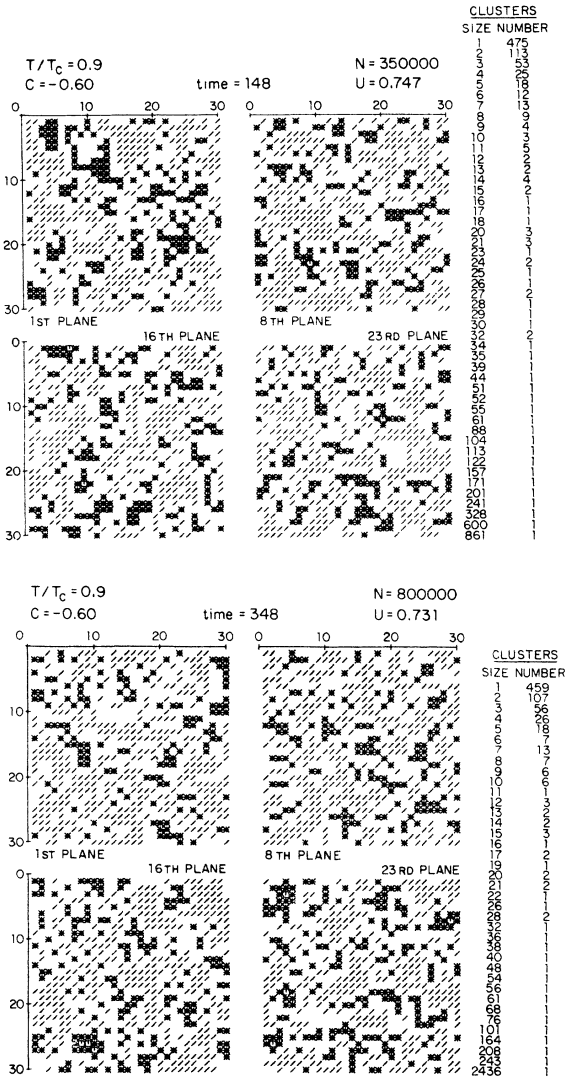

FIG. 7. Same as in Fig. 6 for $T = 0.9T_c$. See Sec. III for details.

a set of intermediate size clusters $10 \lesssim k \lesssim 2000$ which break up and coagulate in an irregular manner with a net tendency to an increase in size. This situation is shown in Fig. 6(a). Little further change is observed in the small cluster distribution throughout our experiment. The number of intermediate size clusters, however, continually decreases with time as the phase segregation proceeds. The large clusters also get noticeably more compact and regular in shape as time goes on. A typical picture of the late state situation is shown in Fig. 6(b).

Pictures for Q_2 are shown in Figs. 7(a) and 7(b). For intermediate times [Fig. 7(a)], no giant cluster is present, but again the small clusters are stabilized quite rapidly. A giant cluster does appear at later times, shown in Fig. 7(b). The clusters in this case however are significantly less compact than for Q_1 at a comparable time. A comparison of Figs. 6(b) and 7(b) also shows that, although in both cases a very big cluster is present (with about 2000 particles), their nature is quite different; for Q_2 the cluster is very loose and resembles more a "percolation" cluster; see also Fig. 5.

Figure 8 shows the picture for Q_3 when the system has more or less reached its equilibrium state. This corresponds, in the lattice-gas language, to a supercritical fluid at a density and temperature where cooperative effects are significant; we expect and find a cluster picture

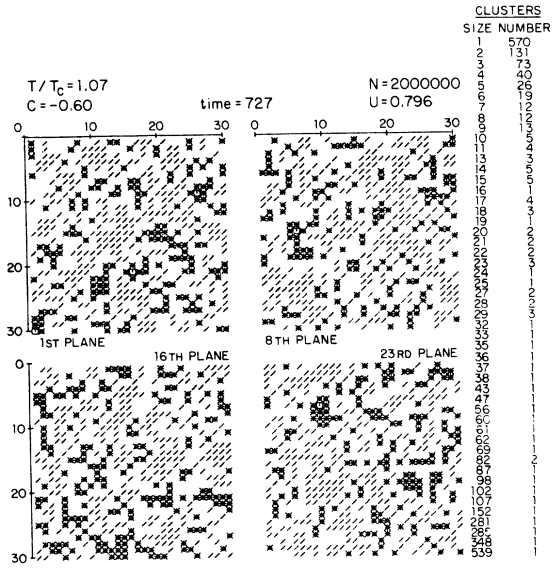

FIG. 8. Same as in Fig. 5 for $T = 1.1T_c$ at a late state in our simulation for comparison with Figs. 6(b) and 7(b).

which is significantly different from what it is at $T = \infty$, when the different sites are independent as in Fig. 5. We note that there is no giant cluster (and this is so even at much later times than the one shown in Fig. 8): the small clusters are still stabilized early, though not as early as in Q_1 or Q_2.

Let us now discuss the clusters in a more quantitative manner. Our first conclusion is that phase segregation has taken place, during the course of our simulation, at the point Q_1. This can be seen very clearly in Fig. 9, where the fraction of particles in clusters of size less or equal than k (denoted by f_k) is plotted against $\log_{10}k$. The flat portion of curve I in Fig. 9 for $10 \lesssim k \lesssim 100$, shows the absence of these clusters in the late time cluster distribution. In terms of the lattice-gas model, this situation corresponds to a well-segregated gas phase comprised of monomers, dimers, etc., and a liquid phase made up of a collection of large clusters resembling liquid droplets. As already mentioned the phase separation at Q_1 takes place on two different time scales: the vapor phase segregates within approximately 10 time units whereas the liquid phase has still not completely consolidated even at the latest time of the simulation (~4000 time units).

To examine whether the distribution for small clusters ($k \lesssim 10$) is indeed similiar to that of a pure gas phase, we performed computer simulation at the coesixtence density ($\bar{n}_A = 0.0146$; $T = 0.59T_c$) marked Q_1' in Fig. 1. Here the system rapidly evolves to its equilibrium state which is made up of small clusters ($k \lesssim 10$) only. The number of clusters of size k, N_k, at these two different concentrations is shown, for small k, in Table IV. Also shown there are the values of the "k-particle cluster partition functions" Z_k at this temperature,[17]

$$Z_k(T) = \sum e^{-\beta E_k}. \tag{5}$$

Here the sum is over all different types of clusters containing k particles and E_k is the (lattice-gas) energy of the cluster which is equal to $4\beta J N_{AA}$, where N_{AA} stands for the number of A-A bonds in the cluster (clusters differing only by a lattice translation are counted as one). $Z_1 = 1$, $Z_2 = 3e^{4\beta J}$, etc. (Our computations for $k \geq 5$ are based on results communicated to us by M. F. Sykes.)

At very low densities, when the clusters are essentially independent, we expect[17] that $N_k \simeq V z^k Z_k(T)$, where V is the volume of the system and z is the fugacity. If this relation held exactly then the ratios $\lambda_k \equiv (N_{k+1}/Z_{k+1})/(N_k/Z_k)$ would be constant and equal to z. Even when cluster interactions are not entirely negligible we still expect[17] that λ_k will be approximately constant and correspond to a "renormalized" fugacity. The values of λ_k for our various cases are shown in Table IV. They are seen to be indeed approximately constant; especially in the equilibrium case, $\bar{n}_A = 0.0146$.

We determine an "effective" value for λ, λ_e, by doing a least-squares fit to the formula for f_k:

$$f_k = N_A^{-1} N_1 \sum_{n=1}^{k} n\lambda^n Z_n, \quad k = 1, \ldots, 10,$$

the fraction of A particles in clusters of size k or less. This gives λ values λ_e which differ slightly

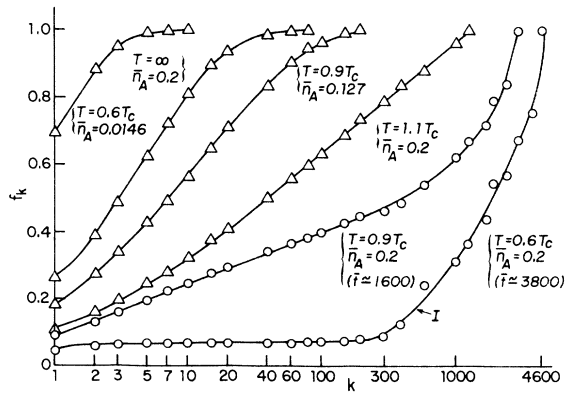

FIG. 9. Size dependence of f_k, the fraction of particles in clusters of size $\leq k$. The triangles correspond to equilibrium states while the circles describe the situation at the values of the time shown.

TABLE IV. Values for Z_k, the k-particle cluster partition functions [see Eq. (5)] and the number of clusters $\bar{N}_k$. The results are averages over different runs (8 when the system was a $30\times30\times30$ lattice and 3 when it was a $50\times50\times50$ lattice; some time averaging was also performed in each case. The standard error of the mean is shown, also the density of clusters λ_k, $\bar{\lambda}$, and λ_e (see Sec. III for details). The value λ_1 was not included in the calculation of λ and λ_e. The case $\bar{n}_A=0.0146$ refers to a $50\times50\times50$ lattice and the values of $\bar{N}_k$ were normalized.

(a) $T=0.6T_c$

k	Z_k	$\bar{n}_A=0.0146$ $\bar{N}_k$	λ_k	$\bar{n}_A=0.20$ $\bar{N}_k$	λ_k
1	1	273.36 ± 0.63	0.0101	227.44 ± 4.08	0.0188
2	13.445 067	37.25 ± 0.27	0.0106	36.00 ± 1.79	0.0134
3	301.283 05	8.89 ± 0.10	0.0107	10.81 ± 0.65	0.0125
4	8681.7083	2.73 ± 0.10	0.0106	3.88 ± 0.40	0.0119
5	282 852	0.97 ± 0.06	0.0102	1.50 ± 0.34	0.0153
6	10 037 271	0.35 ± 0.03	...	0.81 ± 0.18	0.0123
7	377 899 380	0.17 ± 0.02	...	0.38 ± 0.12	...
8	14 890 638	0.03 ± 0.01	...	...	...
9	6 075 549	0.02 ± 0.01	...	...	...
10	$25\,502\,368\times10^6$	...	...	...	...
$z=e^{-12\beta J}=0.0111$		$\lambda_e=0.0103$	$\bar{\lambda}=0.0106$	$\lambda_e=0.0122$	$\bar{\lambda}=0.0131$

(b) $T=0.9T_c$

k	Z_k	$\bar{n}_A=0.127$ $\bar{N}_k$	λ_k	$\bar{n}_A=0.20$ $\bar{N}_k$	λ_k
1	1	621.06 ± 6.37	0.0323	475.04 ± 5.2	0.0302
2	8.1548	163.61 ± 2.15	0.0325	116.96 ± 1.95	0.0320
3	110.836	72.17 ± 2.19	0.0367	50.83 ± 1.60	0.0329
4	1830.894	43.78 ± 1.34	0.0315	27.71 ± 1.16	0.0342
5	336.5853×10^2	25.39 ± 0.99	0.0388	17.42 ± 0.74	0.0348
6	660.1819×10^3	19.33 ± 1.29	0.0357	11.88 ± 0.55	0.0375
7	1354.5203×10^4	14.17 ± 0.55	0.0413	9.13 ± 0.74	0.0351
8	$28\,711.7867\times10^4$	12.39 ± 0.87	0.0337	6.79 ± 0.44	0.0291
9	$623\,883.7193\times10^4$	9.06 ± 0.66	0.0396	4.29 ± 0.41	0.0408
10	$1.382\,24\times10^{11}$	7.94 ± 0.85	...	3.88 ± 0.53	...
$z=e^{-12\beta J}=0.0498$		$\lambda_e=0.0338$	$\bar{\lambda}=0.0362$	$\lambda_e=0.0321$	$\bar{\lambda}=0.0346$

from those obtained by averaging the λ_k, $\bar{\lambda}$ (see Table IV). In the equilibrium case ($\bar{n}_A=0.0146$) we obtain $\lambda_e=0.0103$, which is close, as it should be, to the value of the fugacity, $z=0.0111=e^{-12\beta J}$ on the coexistence line (zero magnetic field). For the clusters in the gas phase at $\bar{n}_A=0.2$, $\lambda_e=0.0122$ which is considerably higher than the value on the coexistence line. This is in accord with our expectations[2,5] since the gas phase at $\bar{n}_A=0.2$ is not in equilibrium with a bulk liquid but rather with relatively small liquid droplets (i.e., clusters of sizes ~1000) which, because of their curvature, will be in equilibrium with a gas at a higher vapor pressure.

A problem arises now however if we want to compute the expected number of monomers. Since $Z_1=1$, we should have, $N_1\simeq V_{\text{vap}}\lambda$, where V_{vap} is the volume (number of sites) belonging to the vapor phase. For $\bar{n}_A=0.0146$, $V_{\text{vap}}=N$, the number of sites in our system and thus $N_1\simeq0.0103\times27\times10^3=278.1$, in agreement with the observations [Table IV(a)]. For $\bar{n}_A=0.2$ we might think at first to use the "lever rule" for obtaining V_{vap}: this gives $V_{\text{vap}}=0.809\times27\times10^3$. This yields however a value for N_1 which is about 20% higher than that observed. We believe that this is again due to the small size of liquid droplets with which the vapor is in equilibrium. It is clear that the layer of lattice sites directly adjacent to the droplets should *not* be counted as part of the volume available to the vapor. An approximate computation of this reduction in V_{vap} (using the sum of s_k for large k as an estimate of the "surface layer") brings the observations in agreement with the theoretical expectations.

The analysis of the cluster distributions at the point Q_2, shown in Fig. 9 and Table IV(b) presents a more difficult problem. As already mentioned the system in this case has not, during the period of our simulation, evolved as far toward its final

equilibrium state as at Q_1. This can be understood as resulting from the fact that the temperature is closer to T_c. This reduces the difference in density between the vapor and liquid phases, or equivalently the difference in the composition of the binary mixture phases. There is a corresponding diminution in the surface tension between the two phases and thus of the force driving the segregation.

Quite aside from this fact, i.e., even if we had continued our simulation to much longer times, the cluster distribution in the gas phase at Q_2' ($\bar{n}_A = 0.127$), extends to much larger clusters, $k \sim 200$, than at Q_1' (see Fig. 9). Hence even after phase segregation has taken place the gap in our cluster distribution at Q_2 would not be so large as at Q_1. Indeed the large gas phase clusters might appear to be small liquid droplets and the physical interpretation of large clusters as liquid droplets becomes now more obscure. We have nevertheless carried out an analysis of the small clusters at Q_2 and compared them with those at Q_2' in the same way as for the lower temperature points [see Table IV(b)]. We find the effective λ values: $\lambda_e = 0.0338$ at Q_2' and $\lambda_e = 0.0321$ at Q_2. Not surprisingly the value of λ at Q_2' differs greatly from the value of the fugacity ($z = 0.0498$) there: the "renormalization" is not small. Note however also that there are large fluctuations (of order 20%) in the values of λ_k, i.e., the cluster distribution is not described well by an "effective" fugacity. The same is true for Q_2. Finally we mention that we do not know the reason that λ at Q_2 is smaller than at Q_2' which is the opposite of what happens at Q_1 and Q_1'. This may again indicate the breakdown of the cluster-droplet analogy at these densities and temperatures.[18] Nevertheless the behavior at Q_2 seems characterized by the existence of small clusters like those of the gas phase. This evidence of phase separation contradicts the conclusion from the structure function (drawn earlier) that Q_2 is outside the spinodal region.

In order to test the extent to which large clusters are (at the late stages of our simulation) compact and thus distinguishable from large "percolation" clusters at infinite temperatures we have plotted in Fig. 10 the "surface"-to-volume ratio s_k/k of clusters of size k vs k. We see there quite clearly, that the larger clusters are considerably more compact at the lower temperatures, especially at $T = 0.6T_c$, than at high temperatures. Nevertheless the actual value of s_k/k for large k (because s_k includes also "internal" A-B bonds it will always be proportional to k as $k \to \infty$) indicates that our clusters are far from having an over-all compact shape. An inspection of the pictures in Fig. 6(b) indicates that although the two-dimensional

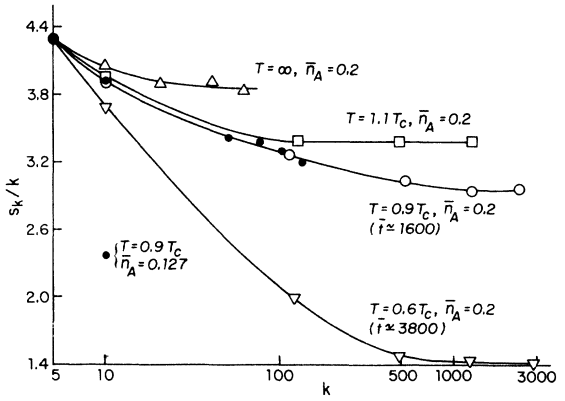

FIG. 10. Size dependence of surface-to-volume ratio s_k/k for typical clusters at "late" times or at equilibrium.

cross sections are compact, the three-dimensional structure is likely to be rather ramified. (The critical density for percolation on the coexistence line is $\bar{n}_A = 0.19$ for the simple cubic lattice and $\bar{n}_A = 0.5$ for the square lattice.[18])

We also note in Fig. 10 that the ratio s_k/k at $T = 0.9T_c$ and $\bar{n}_A = 0.2$ is equal to its value at $\bar{n}_A = 0.127$, on the coexistence line for all clusters of sizes less than about 200. This supports our belief that phase segregation has taken place in this system with the small clusters, $k < 200$, belonging to the gas phase.

IV. TIME EVOLUTION OF CLUSTERS

There are currently several theories[14,19-21] which purport to describe the growth of precipitated "grains" or droplets of the minority phase after quenching. The growth of droplet size with time then depends on the mechanism which is assumed dominant in the phase segregation. In the Lifshitz-Slyozov[19] theory the growth of grains is accomplished primarily by the evaporation of A atoms from one droplet and their deposition on another droplet. This leads (after making various approximations) to an asymptotic behavior in which the volume grows linearly with time: $R^3(t) - R_0^3 \propto t$, where $R(t)$ is some average droplet radius and R_0 is the "initial" value of R. Assuming interfacial control of droplet growth Wagner[20] predicts a linear time dependence for the surface area of the droplets: $R^{3/2}(t) - R_0^{3/2} \propto t$. More recently Binder and Stauffer[14] have developed a model in which the growth of droplets, in the later stages of phase segregation, is due primarily to the diffusion and coagulation of large droplets: they find $R^3(t) \propto t^{1/2}$ in three dimensions at low temperatures (cf. III and review by Binder *et al.* cited in Ref. 2).

TABLE V. Values for the exponents in Eqs. (6) and (7) corresponding to different temperatures, $\bar{n}_A = 0.20$. The values for m and n at $T = 0.6T_c$ seem to evolve in time (see Sec. III for details). The rest of the values are obtained from a fit to the data for $t \gtrsim 100$.

T/T_c	m	n
0.6	0.63 – 0.36	0.11–0.19
0.9	0.10	0.00
1.1	0.04	0.00

It is tempting to interpret our clusters as the droplets in the above theories. This is indeed what we did in II when dealing with a two-dimensional system. There are some difficulties however with this interpretation in the present case. All the above theories assume (explicitly or implicitly) that the grains are compact, approximately spherical, objects. Experimental investigations of grain growth by means of electron microscope studies of thin cross sections (or related methods) are also interpreted in terms of compact droplets. As we have seen however this is not at all the case in our system at the densities we are considering. As already mentioned percolation effects tend to give our clusters a shape which is far from spherical and so their relation to the "experimentally measured" grains is unclear.

While keeping these reservations in mind we have analyzed the temporal behavior of cluster properties in terms of power laws. The average cluster size is

$$\langle k \rangle = \left(\sum_{k \geq 10} k N_k \right) \left(\sum_{k \geq 10} N_k \right)^{-1} \propto t^m . \tag{6}$$

The average "surface/volume" ratio is

$$\left\langle \frac{s}{k} \right\rangle = \left(\sum_{k \geq 10} \frac{sk}{k} \right) \left(\sum_{k \geq 10} N_k \right)^{-1} \propto t^{-n} . \tag{7}$$

In this way we find the exponents in Table V: Figs. 11 and 12 correspond to this analysis.[22]

An inspection of Figs. 11 and 12 shows that the exponent m in Eq. (6) seems to decrease with time, while the exponent n in Eq. (7) increases with time during the late states in our simulation; the two values reported in Table V at $T = 0.6T_c$ correspond respectively to an initial fit for $30 < t < 450$ and to a late one, $t > 450$. This was also the case in III and it may perhaps be interpreted as a change in the dominant mechanism of aggregation or coarsening from that assumed by Binder and Stauffer, or an even slower process, to that assumed by Lifshitz and Slyozov; Binder has given some arguments to explain this apparent

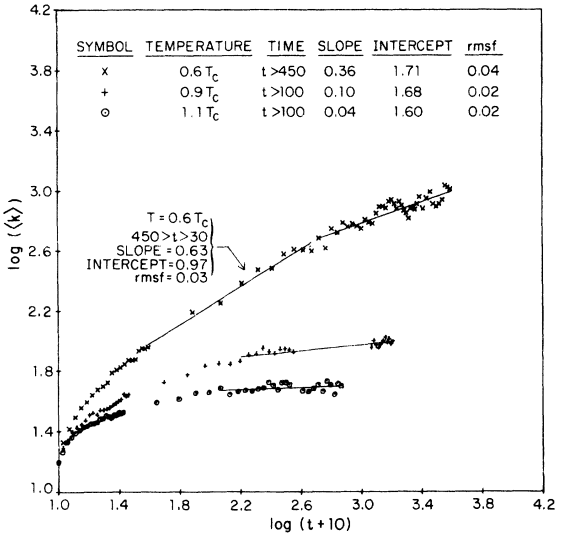

FIG. 11. Time dependence of average cluster size $\langle k \rangle$, where the average is taken over clusters of size $k \geq 10$. The slopes obtained from least-square fits to straight lines are indicated.

crossover.[21] Fitting our data for $\langle k \rangle$ for $t > 30$ we find at $T = 0.6T_c$, $m = 0.49$, which is in very good agreement with the value 0.5 predicted by Binder and Stauffer.[14] We further note that the exponents m and n at Q_2 and Q_3 are much smaller compared to those for Q_1. This shows the difference in the phase separation process at different temperatures once again. It is obvious however that even aside

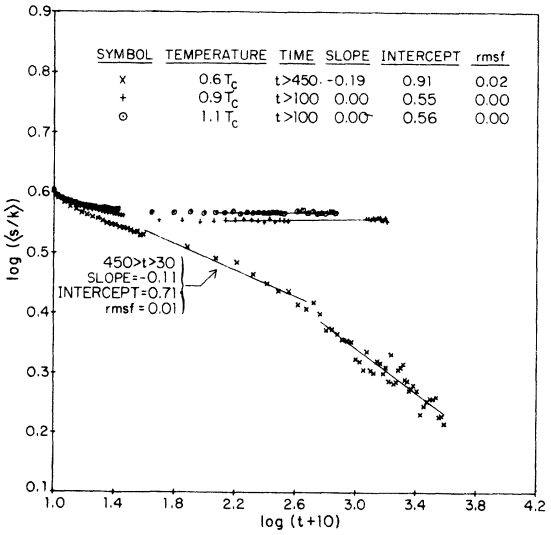

FIG. 12. Time dependence of average surface-to-volume ratio $\langle s/k \rangle$ where the average is taken over clusters of size $k \geq 10$. The slopes obtained from least-square fits to straight lines are indicated.

from the reservations mentioned earlier our data are not sufficiently accurate to determine precise exponents.

V. SUMMARY

The time evolution of the structure function $S(k,t)$, the energy u, and the cluster properties of an A-B alloy containing 20% A atoms have been studied following quenching from an initial random state ($T=\infty$) to different temperatures, $T=0.6T_c$, $0.9T_c$, and $1.1T_c$ (marked by Q_1, Q_2, and Q_3 in Fig. 1). We found that these are qualitatively similar to those of an A-B alloy containing 50% A atoms quenched to $T=0.6T_c$, $1.1T_c$, and $1.5T_c$, respectively (see II and Ref. 13) and much larger than the $S(k,t)$ predicted (at Q_1 and Q_2) by the theory of Langer *et al.*[11] If we adopt the criterion that $S(k,t)$ should not change appreciably for large values of $k(\gtrsim 1/a)$ at late times ($t>100$ time units) if we are outside the "spinodal region," then our results indicate that Q_1 is within the spinodal region, whereas Q_2 is outside.

The phase segregation at Q_1 appears to take place in two separate stages: (i) a "rapid" segregation into a "gas" phase, consisting of clusters of size $k\lesssim 10$, and into "liquid" drops; and (ii) a "slow" growth of the droplets. A clear gap appears in the cluster distribution rather early. The late time distribution of clusters of size $k<10$ at Q_1 is found to be similar to the equilibrium distribution of the pure gas phase at Q_1' (on the coexistence curve at $T=0.59T_c$), when the presence of liquid droplets at Q_1, which changes the fugacity and volume of the gas phase, is properly taken into account. The phase separation process at Q_2 takes place at a much slower pace than at Q_1. It is far from completion even at $t\simeq 1600$ units, in contrast to the situation at Q_1. Yet we believe on the basis of the cluster distribution that here too there has been some segregation into different phases with the clusters making up the liquid phase growing very slowly, in contrast to the conclusion that would be inferred from $S(k,t)$ alone.

Our experiments therefore indicate that the concept of a sharp spinodal line which separates unstable and metastable regions of our system is probably untenable, and that "spinodal-like" behavior extends much closer to the coexistence curve than that predicted by the conventional theories. We are currently carrying on simulations at $T=0.59T_c$ for different densities of A atoms ($\bar{n}_A<0.20$) so that we may understand quantitatively the variation in the kinetics of phase segregation as one proceeds from the spinodal region towards the coexistence curve.

ACKNOWLEDGMENTS

We want to thank J. Langer and D. Stauffer for very valuable comments and help, M. F. Sykes for providing us with the formulas needed for computing $Z_k(T)$ ($k\leq 10$), and O. Penrose for much help with interpreting our cluster distributions.

*Work supported by USAFOSR Grant No. 73-2430B and ERDA Contract No. E(11-1)-3077.

[1]The concept of a spinodal, with reference to fluids, dates back to J. W. Gibbs, in *The Scientific Papers of J. Williard Gibbs* (Dover, New York, 1961). A historical account on this topic with reference to the metallurgical literature is given in the review paper by J. W. Cahn, Trans. AIME (Am. Inst. Min. Metall. Pet. Eng.) 242, 166 (1968).

[2]J. W. Cahn and J. E. Hilliard, J. Chem. Phys. 28, 258 (1958); 31, 688 (1959). For recent reviews, see D. deFontaine, in *Treatise on Solid State Chemistry*, edited by N. B. Hannay (Plenum, New York, 1975), Vol. 5, p. 129; K. Binder, M. H. Kalos, J. L. Lebowitz, and J. Marro, in *Nucleation III*, edited by A. C. Zettlemoyer (Dekker, 1976, to be published). See also the paper by J. W. Cahn listed in Ref. 1.

[3](a) For recent experiments in Zn-Al alloys see K. B. Rundman and J. E. Hilliard, Acta Metall. 15, 1025 (1967); J. Allain, A. Naudon, J. Delafond, A. Junqua, and J. Mimault, Scr. Metall. 8, 831 (1974); A. Naudon, J. Allain, J. Delafond, A. Junqua, and J. Mimault, *ibid.* 8, 1105 (1974); C. D. Clark, S. Messolaras, E. W. J. Mitchell, and R. J. Stewart, J. Appl. Crystallogr. 8, 127 (1975); D. Allen, J. E. Epperson, V. Gerold, G. Kostorz, S. Messolaras, and R. J. Stewart, Conference on Neutron Scattering, Gatlingburgh, Tenn., June 6–10, 1976 (unpublished). Extensive references to earlier works are given in Ref. 2. (b) For recent experiments on binary fluids, see J. S. Huang, W. I. Goldburg, and A. W. Bjerkaas, Phys. Rev. Lett. 32, 921 (1974); for experiments on glasses, see J. W. Cahn and R. J. Charles, Phys. Chem. Glasses 6, 181 (1965); J. Zarzycki and F. Naudin, J. Non-Cryst. Solids 1, 215 (1969); for a recent computer simulation on a Leonard-Jones fluid, see F. F. Abraham, E. Schreiber, M. E. Mruzik, and G. M. Pound, Phys. Rev. Lett. 36, 261 (1976).

[4]For a review on nucleation in solids, see, K. C. Russell, in *Phase Transformation*, edited by H. I. Aaronson (American Society for Metals, Metals Park, Ohio, 1970), p. 219.

[5]See the review article by K. Binder *et al.* listed in Ref. 2. See also H. Reiss, Scr. Metall. 10, 5 (1976); K. Binder and D. Stauffer, Adv. Phys. 25, 343 (1976); C. Domb, J. Phys. A 9, 283 (1976).

[6]A. B. Bortz, M. H. Kalos, J. L. Lebowitz, and M. A. Zendejas, Phys. Rev. B 10, 535 (1974).

[7]J. Marro, A. B. Bortz, M. H. Kalos, and J. L. Lebowitz, Phys. Rev. B 12, 2000 (1975).

[8]M. Rao, M. H. Kalos, J. Marro, and J. L. Lebowitz, Phys. Rev. B 13, 4328 (1976).
[9]C. Domb, in *Phase Transitions and Critical Phenomena*, edited by C. Domb and M. S. Green (Academic, New York, 1974), Vol. 3, p. 357.
[10]D. Amit, Phys. Lett. A 26, 466 (1968); S. Fisk and B. Widom, J. Chem. Phys. 50, 3019 (1969); see also D. Stauffer, Z. Phys. 221, 122 (1969); K. W. Sarkies and N. E. Frankel, Phys. Rev. A 11, 1724 (1975).
[11]J. S. Langer, M. Bar-on, and H. D. Miller, Phys. Rev. A 11, 1417 (1975).
[12]J. W. Essam and M. E. Fisher, J. Chem. Phys. 38, 802 (1963).
[13]J. Marro, Ph. D. thesis (Yeshiva University, New York, 1975) (unpublished).
[14]K. Binder and D. Stauffer, Phys. Rev. Lett. 33, 1006 (1974).
[15]J. A. Baker, Phys. Rev. 129, 99 (1963).
[16]H. J. Leamy, G. H. Gilmer, and K. A. Jackson, Phys. Rev. Lett. 30, 601 (1973).
[17]O. Penrose and J. L. Lebowitz (unpublished); J. L. Lebowitz and O. Penrose, J. Stat. Phys. (to be published).
[18]H. Muller-Krumbhaar, Phys. Lett A 50, 27 (1974); H. Muller-Krumbhaar and E. P. Stoll (unpublished).
[19]I. M. Lifshitz and V. V. Slyozov, J. Phys. Chem. Solids 19, 35 (1961).
[20]C. Wagner, Z. Elektrochem. 65, 581 (1961).
[21]K. Binder (unpublished).
[22]We found a small error in the analysis of $\langle k \rangle$ and $\langle s/k \rangle$ given in Appendix A of Ref. 13. A reanalysis of the relevant data is presented here.